

On the Convergence of Nesterov’s Accelerated Gradient Method in Stochastic Settings

Mahmoud Assran^{1 2 3} Michael Rabbat^{2 3}

Abstract

We study Nesterov’s accelerated gradient method with constant step-size and momentum parameters in the stochastic approximation setting (unbiased gradients with bounded variance) and the finite-sum setting (where randomness is due to sampling mini-batches). To build better insight into the behavior of Nesterov’s method in stochastic settings, we focus throughout on objectives that are smooth, strongly-convex, and twice continuously differentiable. In the stochastic approximation setting, Nesterov’s method converges to a neighborhood of the optimal point at the same accelerated rate as in the deterministic setting. Perhaps surprisingly, in the finite-sum setting, we prove that Nesterov’s method may diverge with the usual choice of step-size and momentum, unless additional conditions on the problem related to conditioning and data coherence are satisfied. Our results shed light as to why Nesterov’s method may fail to converge or achieve acceleration in the finite-sum setting.

1. Introduction

First-order stochastic methods have become the workhorse of machine learning, where many tasks can be cast as optimization problems,

$$\underset{x \in \mathbb{R}^d}{\text{minimize}} f(x). \quad (1)$$

Methods incorporating momentum and acceleration play an important role in the current practice of machine learning (Sutskever et al., 2013; Bottou et al., 2018), where they are commonly used in conjunction with stochastic gradients.

¹Department of Electrical & Computer Engineering, McGill University, Montreal, QC, Canada ²Facebook AI Research, Montreal, QC, Canada ³Mila – Quebec Artificial Intelligence Institute, Montreal, QC, Canada. Correspondence to: Mahmoud Assran <massran@fb.com>, Michael Rabbat <mikerabbat@fb.com>.

However, the theoretical understanding of accelerated methods remains limited when used with stochastic gradients.

This paper studies the *accelerated gradient* (AG) method of Nesterov (1983) with constant step-size and momentum parameters. Given an initial point x_0 , and with $x_{-1} = x_0$, the AG method repeats, for $k \geq 0$,

$$y_{k+1} = x_k + \beta(x_k - x_{k-1}) \quad (2)$$

$$x_{k+1} = y_{k+1} - \alpha g_{k+1}, \quad (3)$$

where α and β are the step-size and momentum parameters, respectively, and in the deterministic setting, $g_{k+1} = \nabla f(y_{k+1})$. When the momentum parameter β is 0, AG simplifies to standard *gradient descent* (GD). When $\beta > 0$ it is possible to achieve accelerated rates of convergence for certain combinations of α and β in the deterministic setting.

1.1. Previous Work with Deterministic Gradients

Suppose that the objective function in (1) is L -smooth and μ -strongly-convex. Then f is minimized at a unique point x^* , and we denote its minimum by $f^* = f(x^*)$. Let $Q := L/\mu$ denote the condition number of f . In the deterministic setting, where $g_k = \nabla f(y_k)$ for all k , GD with constant step-size $\alpha = 2/(L+\mu)$ converges at the rate (Polyak, 1987)

$$f(x_k) - f^* \leq \frac{L}{2} \left(\frac{Q-1}{Q+1} \right)^{2k} \|x_0 - x^*\|^2. \quad (4)$$

The AG method with constant step-size $\alpha = 1/L$ and momentum parameter $\beta = \frac{\sqrt{Q}-1}{\sqrt{Q}+1}$ converges at the rate (Nesterov, 2004)

$$f(x_k) - f^* \leq L \left(\frac{\sqrt{Q}-1}{\sqrt{Q}} \right)^k \|x_0 - x^*\|^2. \quad (5)$$

The rate in (5) matches (up to constants) the tightest-known worst-case lower bound achievable by any first-order black-box method for μ -strongly-convex and L -smooth objectives:

$$f(x_k) - f^* \geq \frac{\mu}{2} \left(\frac{\sqrt{Q}-1}{\sqrt{Q}+1} \right)^{2k} \|x_0 - x^*\|^2. \quad (6)$$

The lower bound (6) is proved in Nesterov (2004) in the infinite dimensional setting under the assumption $Q > 1$.

Accordingly, Nesterov’s Accelerated Gradient method is considered optimal in the sense that the convergence rate in (5) depends on \sqrt{Q} rather than Q .

The proof of (5) presented in Nesterov (2004) uses the method of estimate sequences. Several works have set out to develop better intuition for how the AG method achieves acceleration though other analysis techniques.

One line of work considers the limit of infinitesimally small step-sizes, obtaining ordinary differential equations (ODEs) that model the trajectory of the AG method (Su et al., 2014; Defazio, 2019; Laborde & Oberman, 2019). Allen-Zhu & Orecchia (2014) view the AG method as an alternating iteration between mirror descent and gradient descent and show sublinear convergence of the AG method for smooth convex objectives.

Lessard et al. (2016) and Hu & Lessard (2017) frame the AG method and other popular first-order optimization methods as linear dynamical systems with feedback and characterize their convergence rate using a control-theoretic stability framework. The framework leads to closed-form rates of convergence for strongly-convex quadratic functions with deterministic gradients. For more general (non-quadratic) deterministic problems, the framework provides a means to numerically certify rates of convergence.

1.2. Previous Work with Stochastic Gradients

When Nesterov’s method is run with stochastic gradients g_{k+1} , typically satisfying $\mathbb{E}[g_{k+1}] = \nabla f(y_{k+1})$, we refer to it as the *accelerated stochastic gradient* (ASG) method. In this setting, if $\beta = 0$ then ASG is equivalent to *stochastic gradient descent* (SGD).

Despite the widespread interest in, and use of, the ASG method, there are no definitive theoretical convergence guarantees. Wiegnerinck et al. (1994) study the ASG method in an online learning setting and show that optimization can be modelled as a Markov process but do not provide convergence rates. Yang et al. (2016) study the ASG method in the smooth strongly-convex setting, and show an $\mathcal{O}(1/\sqrt{k})$ convergence rate when employed with a diminishing step-size and bounded gradient assumption, but the rates obtained are slower than those for SGD.

Recent work establishes convergence guarantees for the ASG method in certain restricted settings. Aybat et al. (2019) and Kulunchakov & Mairal (2019a) consider smooth strongly-convex functions in a stochastic approximation model with gradients that are unbiased and have bounded variance, and they show convergence to a neighborhood when running the method with constant step size and momentum. Can et al. (2019) further establish convergence in Wasserstein distribution under a stochastic approximation model. Laborde & Oberman (2019) study a perturbed ODE and show conver-

gence for diminishing step-size. Vaswani et al. (2019) study the ASG method with constant step-size and diminishing momentum, and show linear convergence under a strong-growth condition, where the gradient variance vanishes at a stationary point.

Some results are available for other momentum schemes. Loizou & Richtárik (2017) study Polyak’s heavy-ball momentum method with stochastic gradients for randomized linear problems and show that it converges linearly under an exactness assumption. Gitman et al. (2019) characterize the stationary distribution of the Quasi-Hyperbolic Momentum (QHM) method (Ma & Yarats, 2019) around the minimizer for strongly-convex quadratic functions with bounded gradients and bounded gradient noise variance.

The lack of general convergence guarantees for existing momentum schemes, such as Polyak’s and Nesterov’s, have led many authors to develop alternative accelerated methods specifically for use with stochastic gradients (Lan, 2012; Ghadimi & Lan, 2012; 2013; Allen-Zhu, 2017; Kidambi et al., 2018; Cohen et al., 2018; Kulunchakov & Mairal, 2019b; Liu & Belkin, 2020).

Accelerated first-order methods are also known to be sensitive to inexact gradients when the gradient errors are deterministic (possibly adversarial) and bounded (d’Aspremont, 2008; Devolder et al., 2014).

1.3. Contributions

We provide additional insights into the behavior of Nesterov’s accelerated gradient method when run with stochastic gradients by considering two different settings. We first consider the stochastic approximation setting, where the gradients used by the method are unbiased, conditionally independent from iteration to iteration, and have bounded variance. We show that Nesterov’s method converges at an accelerated linear rate to a region of the optimal solution for smooth strongly-convex quadratic problems.

Next, we consider the finite-sum setting, where $f(x) = \frac{1}{n} \sum_{i=1}^n f_i(x)$, under the assumption that each term f_i is smooth and strongly-convex, and the only randomness is due to sampling one or a mini-batch of terms at each iteration. In this setting we prove that, even when all functions f_i are quadratic, Nesterov’s ASG method with the usual choice of step-size and momentum cannot be guaranteed to converge without making additional assumptions on the condition number and data distribution. When coupled with convergence guarantees in the stochastic approximation setting, this impossibility result illuminates the dichotomy between our understanding of momentum-based methods in the stochastic approximation setting, and practical implementations of these methods in a finite-sum framework.

Our results also shed light as to why Nesterov’s method may

fail to converge or achieve acceleration in the finite-sum setting, providing further insight into what has previously been reported based on empirical observations. In particular, the bounded-variance assumption does not apply in the finite-sum setting with quadratic objectives.

We also suggest choices of the step-size and momentum parameters under which the ASG method is guaranteed to converge for any smooth strongly-convex finite-sum, but where accelerated rates of convergence are no longer guaranteed. Our analysis approach leads to new bounds on the convergence rate of SGD in the finite-sum setting, under the assumption that each term f_i is smooth, strongly-convex, and twice continuously differentiable.

2. Preliminaries and Analysis Framework

In this section we establish a basic framework for analyzing the AG method. Then we specialize it to the stochastic approximation and finite-sum setting settings, respectively, in Sections 3 and 4.

Throughout this paper we assume that f is twice-continuously differentiable, L -smooth, and μ -strongly convex, with $0 < \mu \leq L$; see e.g., Nesterov (2004); Bubeck (2015). Examples of typical tasks satisfying these assumptions are ℓ_2 -regularized logistic regression and ℓ_2 -regularized least-squares regression (i.e., ridge regression). Taken together, these properties imply that the Hessian $\nabla^2 f(x)$ exists, and for all $x \in \mathbb{R}^d$ the eigenvalues of $\nabla^2 f(x)$ lie in the interval $[\mu, L]$. Also, recall that x^* denotes the unique minimizer of f and $f^* = f(x^*)$.

In contrast to all previous work we are aware of, our analysis focuses on the sequence $(y_k)_{k \geq 0}$ generated by the method (2)–(3). Let $r_k := y_k - x^*$ denote the suboptimality of the current iterate, and let $v_k := x_k - x_{k-1}$ denote the velocity.

Substituting the definition of y_{k+1} from (2) into (3) and rearranging, we obtain

$$v_{k+1} = \beta v_k - \alpha g_{k+1}. \quad (7)$$

By using the definition of v_k , substituting (7) and (3) into (2), and rearranging, we also obtain that

$$r_{k+1} = r_k + \beta^2 v_{k-1} - \alpha(1 + \beta)g_k. \quad (8)$$

Combining (7) and (8), we get the recursion

$$\begin{bmatrix} r_{k+1} \\ v_k \end{bmatrix} = \begin{bmatrix} I & \beta^2 I \\ 0 & \beta I \end{bmatrix} \begin{bmatrix} r_k \\ v_{k-1} \end{bmatrix} - \alpha \begin{bmatrix} (1 + \beta)I \\ I \end{bmatrix} g_k. \quad (9)$$

Note that $r_1 = x_0 - x^*$ and $v_0 = 0$ based on the common convention that $x_{-1} = x_0$.

Our analysis below will build on the recursion (9) and will also make use of the basic fact that if $f : \mathbb{R}^d \rightarrow \mathbb{R}$ is twice

continuously differentiable then for all $x, y \in \mathbb{R}^d$

$$\nabla f(y) = \nabla f(x) + \int_0^1 \nabla^2 f(x + t(y-x)) dt (y-x). \quad (10)$$

3. The Stochastic Approximation Setting

Now consider the stochastic approximation setting. We assume, for all k , that g_k is a random vector satisfying

$$\mathbb{E}[g_k] = \nabla f(y_k)$$

and that there is a finite constant σ^2 such that

$$\mathbb{E} \left[\|g_k - \nabla f(y_k)\|^2 \right] \leq \sigma^2.$$

Let $\zeta_k = g_k - \nabla f(y_k)$ denote the gradient noise at iteration k , and suppose that these gradient noise terms are mutually independent. Applying (10) with $y = y_k$ and $x = x^*$, we get that

$$g_k = H_k r_k + \zeta_k, \quad \text{where} \quad H_k = \int_0^1 \nabla^2 f(x^* + t r_k) dt.$$

Using this in (9), we find that r_k and v_k evolve according to

$$\begin{bmatrix} r_{k+1} \\ v_k \end{bmatrix} = A_k \begin{bmatrix} r_k \\ v_{k-1} \end{bmatrix} - \alpha \begin{bmatrix} (1 + \beta)I \\ I \end{bmatrix} \zeta_k, \quad (11)$$

where

$$A_k = \begin{bmatrix} I - \alpha(1 + \beta)H_k & \beta^2 I \\ -\alpha H_k & \beta I \end{bmatrix}. \quad (12)$$

Unrolling the recursion (11), we get that

$$\begin{bmatrix} r_{k+1} \\ v_k \end{bmatrix} = (A_k \cdots A_1) \begin{bmatrix} x_0 - x^* \\ 0 \end{bmatrix} - \alpha \begin{bmatrix} (1 + \beta)I \\ I \end{bmatrix} \zeta_k - \alpha \sum_{j=1}^{k-1} (A_k \cdots A_{j+1}) \begin{bmatrix} (1 + \beta)I \\ I \end{bmatrix} \zeta_j, \quad (13)$$

from which it is clear that we may expect convergence properties to depend on the matrix products $A_k \cdots A_j$.

3.1. The quadratic case

We can explicitly bound the matrix product in the specific case where $f(x) = \frac{1}{2}x^\top Hx - b^\top x + c$, for a symmetric matrix $H \in \mathbb{R}^{d \times d}$, and with $b \in \mathbb{R}^d$ and $c \in \mathbb{R}$. In this case, (13) simplifies to

$$\begin{bmatrix} r_{k+1} \\ v_k \end{bmatrix} = A^k \begin{bmatrix} x_0 - x^* \\ 0 \end{bmatrix} - \alpha \sum_{j=1}^k A^{k-j} \begin{bmatrix} (1 + \beta)I \\ I \end{bmatrix} \zeta_j, \quad (14)$$

where

$$A = \begin{bmatrix} I - \alpha(1 + \beta)H & \beta^2 I \\ -\alpha H & \beta I \end{bmatrix}. \quad (15)$$

We obtain an error bound by ensuring that the spectral radius $\rho(A)$ of A is less than 1. In this case we recover the well-known rate for AG in the deterministic setting. Let $\Delta_\lambda = (1 + \beta)^2(1 - \alpha\lambda)^2 - 4\beta(1 - \alpha\lambda)$ and define

$$\rho_\lambda(\alpha, \beta) = \begin{cases} \frac{1}{2} |(1 + \beta)(1 - \alpha\lambda)| + \frac{1}{2} \sqrt{\Delta_\lambda} & \text{if } \Delta_\lambda \geq 0, \\ \sqrt{\beta(1 - \alpha\lambda)} & \text{otherwise.} \end{cases}$$

Theorem 1. *Let $\rho(\alpha, \beta) = \max\{\rho_\mu(\alpha, \beta), \rho_L(\alpha, \beta)\}$. If α and β are chosen so that $\rho(\alpha, \beta) < 1$, then for any $\epsilon > 0$, there exists a constant C_ϵ such that, for all k ,*

$$\mathbb{E} \left[\|y_{k+1} - x^*\|^2 \right] \leq C_\epsilon \left((\rho(\alpha, \beta) + \epsilon)^{2k} \|x_0 - x^*\|^2 + \frac{\alpha^2((1 + \beta)^2 + 1)}{1 - \rho(\alpha, \beta)^2} \sigma^2 \right).$$

Theorem 1 holds with respect to all norms; the constant C_ϵ depends on ϵ and the choice of norm. Theorem 1 shows that ASG converges at a linear rate to a neighborhood of the minimizer of f that is proportional to σ^2 . The proof is given in Appendix A of the supplementary material, and we provide numerical experiments in Section 3.2 to analyze the tightness of the convergence rate and coefficient multiplying σ^2 in Theorem 1. Comparing to Aybat et al. (2019), we recover the same rate, despite taking a different approach, and the coefficient multiplying σ^2 in Theorem 1 is smaller.

Corollary 1.1. *Suppose that $\alpha = 1/L$ and $\beta = \frac{\sqrt{Q}-1}{\sqrt{Q}+1}$. Then for and all k ,*

$$\mathbb{E}[f(y_{k+1})] - f^* \leq \frac{L}{2} \left(\frac{\sqrt{Q}-1}{\sqrt{Q}} + \epsilon_k \right)^{2k} \|x_0 - x^*\|^2 + C_\epsilon \frac{5Q^2 + 2Q^{3/2} + Q}{2L(2\sqrt{Q}-1)(\sqrt{Q}+1)^2} \sigma^2,$$

where $\epsilon_k \sim (\sqrt[k]{k} - 1)$.

Theorem 2. *Let f be L -smooth, μ -strongly-convex, and twice continuously-differentiable (not necessarily quadratic). Suppose that $\alpha = 2/(\mu+L)$ and $\beta = 0$. Then for all k ,*

$$\mathbb{E}[f(y_{k+1})] - f^* \leq \frac{L}{2} \left(\frac{Q-1}{Q+1} \right)^{2k} \|x_0 - x^*\|^2 + \frac{Q\sigma^2}{2L}.$$

Corollary 1.1 confirms that, with the standard choice of parameters, ASG converges at an accelerated rate to a region of the optimizer. Comparing with Theorem 2, which is proved in Appendix B, we see that in the stochastic approximation setting, with bounded variance, ASG not only converges at a faster rate than SGD, the factor multiplying σ^2 also scales more favorably, $\mathcal{O}(\sqrt{Q}\sigma^2)$ for ASG vs. $\mathcal{O}(Q\sigma^2)$ for SGD.

3.2. Numerical Experiments

In Figure 1 we visualize runs of the ASG method on a least-squares regression problem for different problem condition numbers Q . The objective f corresponds to the worst-case quadratic function used to construct the lower bound (6) (Nesterov, 2004), for dimension $d = 100$. Stochastic gradients are sampled by adding zero-mean Gaussian noise with variance $\sigma^2 = 0.0025$ to the true gradient. The left plots in each sub-figure depict theoretical predictions from Theorem 1, while the right plots in each sub-figure depict empirical results. Each pixel corresponds to an independent run of the ASG method for a specific choice of constant step-size and momentum parameters. In all figures, the area enclosed by the red contour depicts the theoretical stability region from Theorem 1 for which $\rho(\alpha, \beta) < 1$.

Figures 1a/1c/1e showcase the coefficient multiplying the variance term, which is taken to be $\frac{\alpha^2((1+\beta)^2+1)}{1-\rho(\alpha,\beta)^2}$ in theory. Brighter regions correspond to smaller coefficients, while darker regions correspond to larger coefficients. All sets of figures (theoretical and empirical) use the same color scale. We can see that the coefficient of the variance term in Theorem 1 provides a good characterization of the magnitude of the neighbourhood of convergence. The constant C_ϵ is approximated as $1 + (1 - \rho(\alpha, \beta)^2)(\|A\|^2 - \rho(\alpha, \beta)^2)$, where $\|A\|$ denotes the largest singular value of A in (15), and $\rho(\alpha, \beta)$ is the largest eigenvalue of A . More detail on this simple approximation is provided in Appendix A.1 of the supplementary material.

Figures 1b/1d/1f showcase the linear convergence rate in theory and in practice. Brighter regions correspond to faster rates, and darker regions correspond to slower rates. Again, all figures (theoretical and empirical) use the same color scale. We can see that the theoretical linear convergence rates in Theorem 1 provide a good characterization of the empirical convergence rates. Moreover, the theoretical conditions for convergence in Theorem 1 depicted by the red-contour appear to be tight.

In short, the theory developed in this section appears to provide an accurate characterization of the ASG method in the stochastic-approximation setting. As we will see in the subsequent section, this theoretical characterization does not reflect its behavior in the finite-sum setting, which is typically closer to practical machine-learning setups, where randomness is due to mini-batching.

4. The Finite-Sum Setting

Now consider the finite-sum setting, with

$$f(x) = \frac{1}{n} \sum_{i=1}^n f_i(x), \quad (16)$$

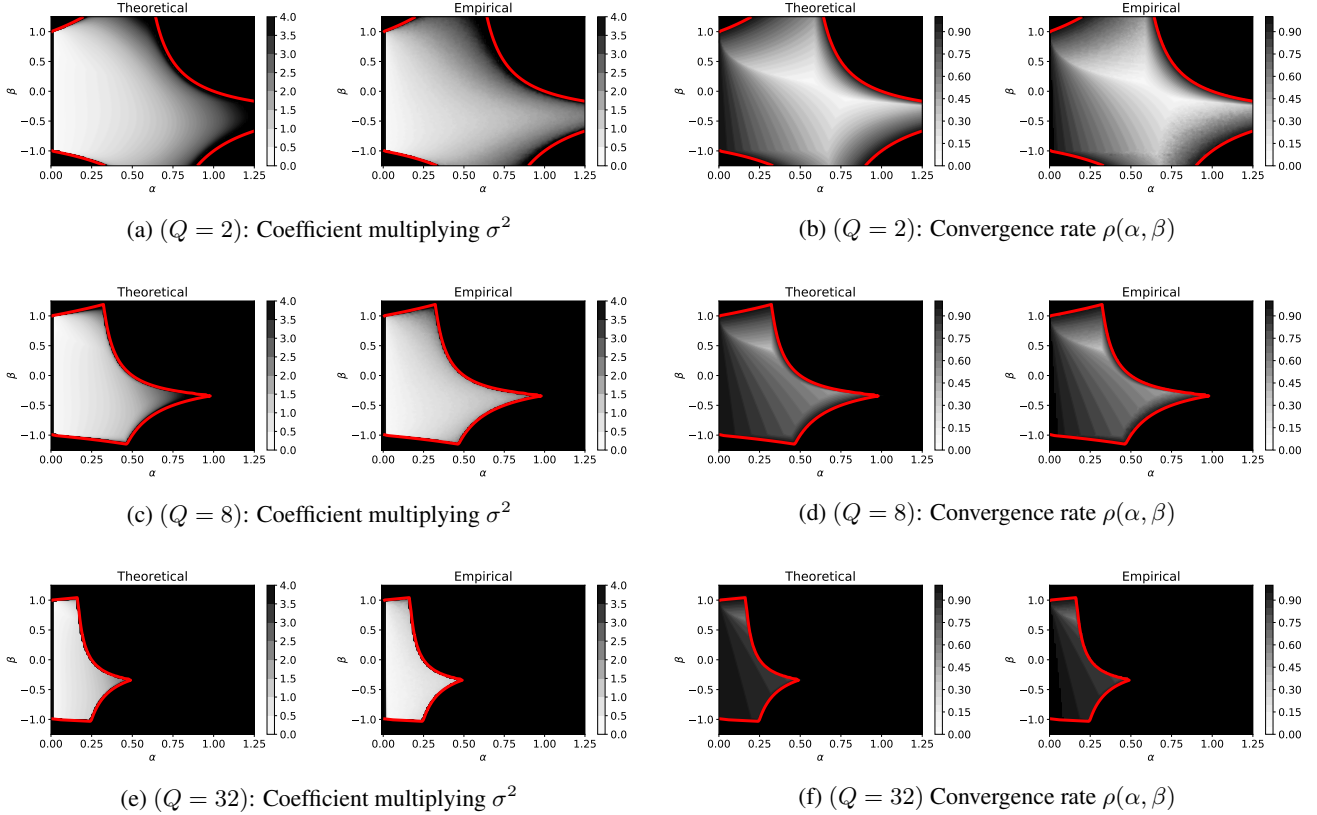


Figure 1. Visualizing the accuracy with which the theory predicts the coefficient of the variance term and the convergence rate for different choices of constant step-size and momentum parameters, and various objective condition numbers Q . Plots labeled “Theoretical” depict theoretical results from Theorem 1. Plots labeled “Empirical” depict empirical results when using the ASG method to solve a least-squares regression problem with additive Gaussian noise; each pixel corresponds to an independent run of the ASG method for a specific choice of constant step-size and momentum parameters. In all figures, the area enclosed by the red contour depicts the theoretical stability region from Theorem 1 for which $\rho(\alpha, \beta) < 1$. Fig. 1a/1c/1e: Pixel intensities correspond to the coefficient of the variance term in Theorem 1 ($\lim_{k \rightarrow \infty} \frac{1}{\sigma} \mathbb{E} \|y_k - x^*\|_\infty$), which provides a good characterization of the magnitude of the neighbourhood of convergence, even without explicit knowledge of the constant C_ϵ . Brighter regions correspond to smaller coefficients, while darker regions correspond to larger coefficients. Fig. 1b/1d/1f: Pixel intensities correspond to the theoretical convergence rates in Theorem 1, which provides a good characterization of the empirical convergence rates. Brighter regions correspond to faster rates, and darker regions correspond to slower rates. The theoretical conditions for convergence in Theorem 1 depicted by the red-contour are tight.

where each function f_i is μ -strongly convex, L -smooth, and twice continuously differentiable. In this setting, stochastic gradients g_k are obtained by sampling a subset of terms. This can be seen as approximating the gradient $\nabla f(y_k)$ with a mini-batch gradient

$$g_k = \sum_{i=1}^n \nu_{k,i} \nabla f_i(y_k), \quad (17)$$

where $\nu_k \in \mathbb{R}^n$ is a sampling vector with components $\nu_{k,i}$ satisfying $\mathbb{E}[\nu_{k,i}] = \frac{1}{n}$ (Gower et al., 2019). To simplify the discussion, let us assume that the mini-batch sampled at every iteration k has the same size, and all elements are given the same weight, so $\sum_{i=1}^n \nu_{k,i} = 1$, those indices i which are sampled have $\nu_{k,i} = \frac{1}{m}$ where m is the mini-batch size ($1 \leq m \leq n$), and $\nu_{k,i} = 0$ for all other indices.

4.1. An Impossibility Result

Next we show that even when each function f_i is well-behaved, the ASG method may diverge when using the standard choice of step-size and momentum. Instability of Nesterov’s method for convex (but not strongly convex) functions with unbounded eigenvalues is shown in Liu & Belkin (2020). This section employs a different proof technique to strengthen this result to the case where each function f_i is μ -strongly-convex and L -smooth (all eigenvalues bounded between μ and L).

Let us assume that we do not see the same mini-batch twice consecutively; i.e.,

$$\mathbb{P}(\|\nu_{k+1} - \nu_k\| > 0) = 1 \quad \text{for all } k. \quad (18)$$

It is typical in practice to perform training in epochs over the data set, and to randomly permute the data set at the beginning of each epoch, so it is unlikely to see the same mini-batch twice in a row. Note we have not assumed that the sample vectors ν_k are independent. We do assume that $\mathbb{E}_k[\nu_{k,i}] = \frac{1}{n}$, where \mathbb{E}_k denotes expectation with respect to the marginal distribution of ν_k .

The *interpolation condition* is said to hold if the minimizer x^* of f also minimizes each f_i ; i.e., if $\nabla f_i(x^*) = 0$ for all $i = 1, \dots, n$. It has been observed in some settings that stronger convergence guarantees can also be obtained when interpolation or a related assumption holds; e.g., (Schmidt & Le Roux, 2013; Loizou & Richtárik, 2017; Ma et al., 2018; Vaswani et al., 2019).

Theorem 3. *Suppose we run the ASG method (2)–(3) in a finite-sum setting where $n \geq 3$ and the sampling vectors ν_k satisfy the condition (18). For any initial point $x_0 \in \mathbb{R}^d$, there exist L -smooth, μ -strongly convex quadratic functions f_1, \dots, f_n such that f is also L -smooth and μ -strongly convex, and if we run the ASG method with $\alpha = 1/L$ and $\beta = \frac{\sqrt{Q}-1}{\sqrt{Q}+1}$, then*

$$\lim_{k \rightarrow \infty} \mathbb{E}[\|y_k - x^*\|] = \infty.$$

This is true even if the functions f_1, \dots, f_n are required to satisfy the interpolation condition.

Proof. We will prove this claim constructively. Given the initial vector x_0 , choose $x^* \in \mathbb{R}^d$ to be any vector $x^* \neq x_0$.

Let U be an orthogonal matrix. Let the Hessian matrices H_i , $i = 1, \dots, n$, be chosen so that they are all diagonalized by U , and let Λ_i denote the diagonal matrix of eigenvalues of H_i ; i.e., $H_i = U\Lambda_iU^\top$. Denote by Λ_{ν_k} the matrix

$$\Lambda_{\nu_k} = \sum_{i=1}^n \nu_{k,i} \Lambda_i. \quad (19)$$

It follows that $\Lambda_{\nu_k} \in \mathbb{R}^{d \times d}$ is also diagonal, and all of its diagonal entries are in $[\mu, L]$.

Recall that we have assumed that the functions f_i are quadratic: $f_i(x) = \frac{1}{2}x^\top H_i x - b_i^\top x + c_i$. Let us assume that $b_i \in \mathbb{R}^d$ and $c_i \in \mathbb{R}$ are chosen so that all functions f_i are minimized at the same point x^* , satisfying the interpolation condition. Then from (10), we have

$$g_k = U\Lambda_{\nu_k}U^\top r_k. \quad (20)$$

Using this in (9) and unrolling, we obtain that

$$\begin{bmatrix} r_{k+1} \\ v_k \end{bmatrix} = A_k A_{k-1} \dots A_1 \begin{bmatrix} r_1 \\ v_0 \end{bmatrix}, \quad (21)$$

where

$$A_j = \begin{bmatrix} I - \alpha(1 + \beta)U\Lambda_{\nu_j}U^\top & \beta^2 I \\ -\alpha U\Lambda_{\nu_j}U^\top & \beta I \end{bmatrix}. \quad (22)$$

For fixed n and m , there are a finite number of sampling vectors ν_k (precisely $\binom{n}{m}$), and therefore the matrices A_j belong to a bounded set \mathcal{A} . It follows that the trajectory $([r_{k+1}, v_k]^\top)_{k \geq 0}$ is stable if the joint spectral radius of the set of matrices \mathcal{A} is less than one (Rota & Strang, 1960). Conversely, if $\mathbb{E}[\rho(A_k \dots A_1)^{1/k}] > 1$ for all k sufficiently large, then $\lim_{k \rightarrow \infty} \|y_k - x^*\| = \infty$.

Based on the construction above, the norm of the matrix product $A_k \dots A_1$ in (21) can be characterized by studying products of smaller 2×2 matrices of the form

$$B(\lambda_{k,j}) = \begin{bmatrix} 1 - \alpha(1 + \beta)\lambda_{k,j} & \beta^2 \\ -\alpha\lambda_{k,j} & \beta \end{bmatrix}, \quad (23)$$

where $\lambda_{k,j}$ is a diagonal entry of Λ_{ν_k} . To see this, observe that there is a permutation matrix $P \in \{0, 1\}^{2d \times 2d}$ such that (see Appendix C)

$$\begin{aligned} P \begin{bmatrix} U^\top & 0 \\ 0 & U^\top \end{bmatrix} A_j \begin{bmatrix} U & 0 \\ 0 & U \end{bmatrix} P^\top \\ = \begin{bmatrix} B(\lambda_{j,1}) & 0 & \dots & 0 \\ 0 & B(\lambda_{j,2}) & \dots & 0 \\ \vdots & \vdots & \ddots & \vdots \\ 0 & 0 & \dots & B(\lambda_{j,d}) \end{bmatrix}, \end{aligned}$$

where $\lambda_{j,i}$ is the i th diagonal entry of Λ_{ν_j} .

Furthermore, since all matrices H_i have the same eigenvectors, we have that

$$\begin{aligned} P \begin{bmatrix} U^\top & 0 \\ 0 & U^\top \end{bmatrix} A_k A_{k-1} \dots A_1 \begin{bmatrix} U & 0 \\ 0 & U \end{bmatrix} P^\top \\ = \begin{bmatrix} T_{k,1} & 0 & \dots & 0 \\ 0 & T_{k,2} & \dots & 0 \\ \vdots & \vdots & \ddots & \vdots \\ 0 & 0 & \dots & T_{k,d} \end{bmatrix}, \end{aligned}$$

where $T_{k,j} = B(\lambda_{k,j}) \dots B(\lambda_{1,j})$. Hence, the spectral radius of the product $A_k \dots A_1$ corresponds to the maximum spectral radius of any of the 2×2 matrices $T_{k,j}$, $j = 1, \dots, d$.

Let j index a subspace such that $u_j^\top r_1 \neq 0$, where u_j is the j th column of U . To simplify the discussion, suppose that all mini-batches are of size $m = 1$, and assume $n > 1$. Since we can define the Hessians of the functions f_i such that the eigenvalues pair together arbitrarily, consider matrix products of the form

$$T_{k,j} = B(L)B(\mu)^{k_1}B(L)B(\mu)^{k_2} \dots B(L)B(\mu)^{k_s}, \quad (24)$$

where $k = k_1 + \dots + k_s + s$. That is, all but one of the functions f_i have the eigenvalue μ in this subspace, and the remaining one has eigenvalue L in this subspace. Hence, most of the time we sample mini-batches corresponding to $B(\mu)$,

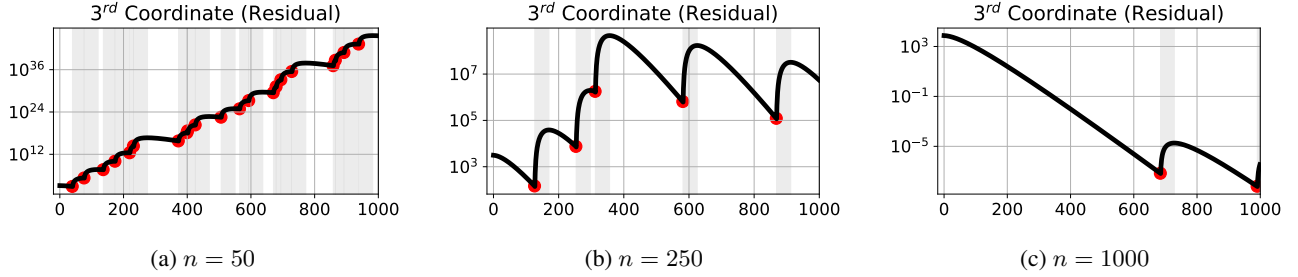


Figure 2. Visualizing the convergence of Nesterov's ASG method $y_k - x^*$ in \mathbb{R}^3 along a single coordinate direction in the L -smooth μ -strongly-convex finite-sum setting with the usual choice of parameters ($\alpha = 1/L$ and $\beta = (\sqrt{Q}-1)/(\sqrt{Q}+1)$). The L -smoothness parameter is 100 and the modulus of strong-convexity μ is 0.05. There are n functions f_1, \dots, f_n in the finite-sum, each with the same minimizer x^* . All the functions have the eigenvalue L along the first coordinate basis vector, and the eigenvalue μ along the second coordinate basis vector. Along the third coordinate basis vector, the functions f_1, \dots, f_{n-1} have eigenvalue μ , while only a single function, f_n , has eigenvalue L . At each iteration, the ASG method obtains a stochastic gradient by sampling one function from the finite-sum. Red points indicate iterations at which the mini-batch corresponding to the function f_n was sampled. Gray shading indicates iterations at which the momentum and gradient vector point in opposite directions along the given coordinate axis. The inconsistent mini-batch leads to the divergence of the ASG method, but becomes less destabilizing as the number of terms in the finite-sum n grows.

and once in a while we sample mini-batches with $B(L)$. Moreover, since we do not sample the same mini-batch twice consecutively, we never see back-to-back $B(L)$'s. For this case, and with the standard choice of step-size and momentum parameters, we can precisely characterize the spectral radius of $T_{k,j}$.

Lemma 1. *If $\alpha = 1/L$ and $\beta = \frac{\sqrt{Q}-1}{\sqrt{Q}+1}$, then*

$$\rho(T_j) = \left(\frac{\sqrt{Q}-1}{\sqrt{Q}} \right)^k \times k_1 \cdots k_s.$$

The proof of Lemma 1 is given in Appendix D. Since we do not sample the same mini-batch twice in a row, it follows that $k_j \geq 1$ for all $j = 1, \dots, s$. Based on the assumption that $\mathbb{E}_k[\nu_{k,i}] = \frac{1}{n}$, we have $\mathbb{E}[s] = \frac{k}{n}$. Moreover, since $\mathbb{E}_k[\nu_{k,i}] = \frac{1}{n}$, for large k ($\gg n$) we have $\mathbb{E}[(k_1 \cdots k_s)^{\frac{1}{k}}] \approx (n-1)^{1/n}$. Thus, for sufficiently large Q and sufficiently large k ,

$$\mathbb{E}[\rho(A_k \cdots A_1)^{1/k}] > 1.$$

Therefore, $\lim_{k \rightarrow \infty} \mathbb{E} \|y_k - x^*\| = \infty$.

Recall that we assumed the interpolation condition holds in order to get g_k of the form (20). If we relax this and do not require interpolation, then g_k will have an additional term involving $\nabla f_i(x^*)$, and the expression (21) will also have an additional terms, akin to the ζ_k terms in (13). The same arguments still apply, leading to the same conclusion. \square

4.2. Example

The divergence result in Theorem 3 stems from the fact that the algorithm acquires momentum along a low-curvature

direction, and then, suddenly, a high-curvature mini-batch is sampled that overshoots along the current trajectory. Momentum prevents the iterates from immediately adapting to the overshoot, and propels the iterates away from the minimizer for several consecutive iterations.

To illustrate this effect, consider the following example finite-sum problem with $d = 3$, where each function f_i is a strongly-convex quadratic with gradient

$$\nabla f_i(x) = U \Lambda_i U^T (x - x^*).$$

For simplicity, take $U = I$, and let

$$\Lambda_i = \begin{bmatrix} L & 0 & 0 \\ 0 & \mu & 0 \\ 0 & 0 & \lambda_i \end{bmatrix}.$$

The scalar λ_i is equal to μ for all $i \neq n$, and is equal to L for $i = n$. Therefore, each function f_i is μ -strongly convex, L -smooth, and minimized at x^* , and the global objective f is also μ -strongly convex, L -smooth, and minimized at x^* . Moreover, the functions f_i are nearly all identical, except for f_n , which we refer to as the inconsistent mini-batch.

From the proof of Theorem 3, the growth rate of the iterates along the third coordinate direction, with the usual choice of parameters ($\alpha = 1/L$, $\beta = \frac{\sqrt{Q}-1}{\sqrt{Q}+1}$), is

$$\mathbb{E}[\rho(A_k \cdots A_1)^{1/k}] \sim \left(\frac{\sqrt{Q}-1}{\sqrt{Q}} \right) (n-1)^{\frac{1}{n}}.$$

Notice that the term $(n-1)^{\frac{1}{n}}$ goes to 1 as n grows to infinity. Hence, for a fixed condition number Q , the ASG method exhibits an increased probability of convergence as

n becomes large. The intuition for this is that we sample the inconsistent mini-batch less frequently, and thereby decrease the likelihood of derailing convergence.

Figure 2 illustrates the convergence of the ASG method in this setting with the usual choice of parameters ($\alpha = 1/L$, $\beta = \frac{\sqrt{Q}-1}{\sqrt{Q}+1}$), for various n (number of terms in the finite-sum). At each iteration, the ASG method obtains a stochastic gradient by sampling a mini-batch from the finite-sum. Components of iterates along the first coordinate direction converge in a finite number of steps, and components of iterates along the second coordinate direction converge at Nesterov's rate $(\sqrt{Q}-1)/\sqrt{Q}$. Meanwhile, components of iterates along the third coordinate direction diverge.

Annotated red points indicate iterations at which the mini-batch corresponding to the function f_n was sampled. The shaded windows illustrate that immediately after the inconsistent mini-batch is sampled, the gradient and momentum buffer have opposite signs for several consecutive iterations.

4.3. Convergent Parameters

Next we turn our attention to finding alternative settings for the parameters α and β in the ASG method which guarantee convergence in the finite-sum setting. Vaswani et al. (2019) obtain linear convergence under a strong growth condition using an alternative formulation of ASG which has multiple momentum parameters by keeping the step-size constant and having the momentum parameters vary. Here we focus on constant step-size and momentum and make no assumptions about growth.

Our approach is to bound the spectral norm of the products $\|A_k \cdots A_j\|$ using submultiplicativity of matrix norms. This recovers linear convergence to a neighborhood of the minimizer, but the rate is no longer accelerated.

Define the quantities

$$\begin{aligned} C_\lambda(\alpha, \beta) &= (1 - \alpha(1 + \beta)\lambda)^2 + \alpha^2\lambda^2 + \beta^2(\beta^2 + 1) \\ \tilde{\Delta}_\lambda(\alpha, \beta) &= C_\lambda(\alpha, \beta)^2 - 4\beta^2(1 - \alpha\lambda)^2 \\ R_\lambda(\alpha, \beta) &= \frac{1}{\sqrt{2}} \left(C_\lambda(\alpha, \beta) + \sqrt{\tilde{\Delta}_\lambda(\alpha, \beta)} \right)^{1/2} \end{aligned}$$

and let $R(\alpha, \beta) = \max_{\lambda \in [\mu, L]} R_\lambda(\alpha, \beta)$.

Theorem 4. *Let α and β be chosen so that $R(\alpha, \beta) < 1$. Then for all $k \geq 0$,*

$$\begin{aligned} \mathbb{E} \|y_{k+1} - x^*\| &\leq R(\alpha, \beta)^k \|y_1 - x^*\| \\ &\quad + \frac{\alpha\sqrt{(1 + \beta)^2 + 1}}{1 - R(\alpha, \beta)}\sigma, \end{aligned}$$

where

$$\sigma = \frac{1}{n} \sum_{i=1}^n \|\nabla f_i(x^*)\|.$$

Theorem 4 is proved in Appendix E for general L -smooth μ -strongly-convex functions. Note that if an interpolation condition holds (a weaker assumption than the strong growth condition), then $\sigma = 0$.

Theorem 4 shows that the ASG method can be made to converge in the finite-sum setting for L -smooth μ -strongly convex objective functions when run with constant step-sizes. In particular, the algorithm converges at a linear rate to a neighborhood of the minimizer that is proportional to the variance of the noise terms. Note that this theorem also allows for negative momentum parameters. Using the spectral norm to guarantee stability is restrictive, in that it is sufficient but not necessary. There may be values of α and β for which $R(\alpha, \beta) \geq 1$ and the algorithm still converges. Having $R(\alpha, \beta) < 1$ ensures that $\|r_k\| + \|v_k\|$ decreases at every iteration.

Corollary 4.1. *Suppose that $\alpha < \frac{2}{L}$ and $\beta = 0$. Then for all $k \geq 0$*

$$\mathbb{E} \|y_k - x^*\| \leq \varrho(\alpha)^k \|y_0 - x^*\| + \frac{\alpha}{1 - \varrho(\alpha)}\sigma,$$

where $\varrho(\alpha) := \max_{\lambda \in \{\mu, L\}} |1 - \alpha\lambda|$.

Corollary 4.1 is proved in Appendix F for smooth strongly-convex functions, and shows the convergence of SGD in the finite-sum setting without making any assumptions on the noise distribution.

Corollary 4.2. *Suppose that $\alpha = \frac{2}{\mu+L}$ and $\beta = 0$. Then for all $k \geq 0$*

$$\mathbb{E} \|y_k - x^*\| \leq \left(\frac{Q-1}{Q+1} \right)^k \|y_0 - x^*\| + \frac{1}{\mu}\sigma.$$

Corollary 4.2, is proved in Appendix F for smooth strongly-convex functions, and shows that SGD converges to a neighborhood of x^* at the same linear rate as GD, viz. (4), in the finite-sum setting, without making any assumptions on the noise distribution, such as the strong-growth condition; a novel result to the best of our knowledge. Moreover, when the interpolation condition holds, we have that $\sigma = 0$.

Figure 3 illustrates the tightness of the convergence rate and variance bound in Corollary 4.2 when minimizing randomly generated least-squares problems with various condition numbers. The finite-sum least-squares problem consists of 25000 data samples, with 2 features each, partitioned into 50 mini-batches, each with condition number Q . At each iteration, one of the 50 mini-batches is sampled to compute a stochastic gradient step. Dashed lines indicate the theoretical convergence rate and variance bound from Corollary 4.2. Solid lines indicate the empirical convergence observed in practice. The convergence rate and variance bound in Corollary 4.2 provide a tight characterization of the SGD convergence observed in practice.

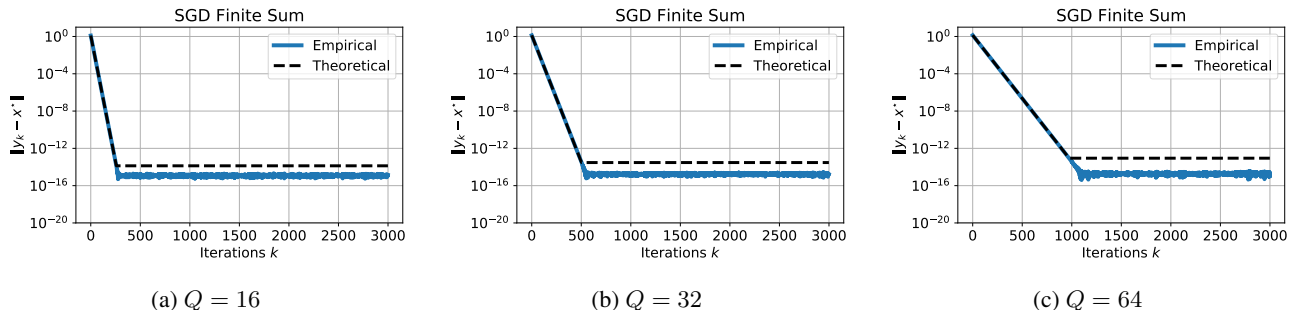


Figure 3. Visualizing the accuracy with which Corollary 4.2 predicts the theoretical convergence of SGD with step-size $\alpha = 2/(\mu+L)$ in the finite-sum setting, when minimizing randomly generated least-squares problems with various condition numbers Q . The finite-sum problem consists of 25000 data samples, with 2 features each, partitioned into 50 mini-batches, each with condition number Q . At each iteration one of the 50 mini-batches is sampled to compute a stochastic gradient step. Dashed lines indicate the theoretical convergence rate and variance bound from Corollary 4.2. Solid lines indicate the empirical convergence observed in practice. The convergence rate and variance bound in Corollary 4.2 is tight.

5. Conclusions

This paper contributes to a broader understanding of the ASG method in stochastic settings. Although the method behaves well in the stochastic approximation setting, it may diverge in the finite-sum setting when using the usual step-size and momentum. This emphasizes the important role the bounded variance assumption plays in the stochastic approximation setting, since a similar condition does not necessarily hold in the finite-sum setting. Forsaking acceleration guarantees, we provide conditions under which the ASG method is guaranteed to converge in the smooth strongly-convex finite-sum setting with constant step-size and momentum, without assuming any growth or interpolation condition.

We believe there is scope to obtain tighter convergence bounds for the ASG method with constant step-size and momentum in the finite-sum setting. Convergence guarantees using the joint spectral radius are likely to provide the tightest and most intuitive bounds, but are also difficult to obtain. To date, Lyapunov-based proof techniques have been the most fruitful in the literature.

We also believe that there is scope to improve the robustness of Nesterov’s method to inconsistent mini-batches in the finite-sum setting. For example, adaptive restarts, which have been shown to improve the convergence rate of Nesterov’s method (O’Donoghue & Candès, 2015) with deterministic gradients, may also be able to mitigate the divergence behaviour identified in this paper.

We also believe that future work understanding the role that negative momentum parameters play in practice may lead to improved optimization of machine learning models. All convergence guarantees and variance bounds in this paper hold for both positive and negative momentum parameters.

Our variance bounds and theoretical rates support the observation that negative momentum parameters may slow-down convergence, but can also lead to non-trivial variance reduction. Previous work has found negative momentum to be useful in asynchronous distributed optimization (Mitliagkas et al., 2016) and for stabilizing adversarial training (Gidel et al., 2018). Although it is almost certainly not possible (in general) to obtain zero variance solutions by only using negative momentum parameters, for Deep Learning practitioners that already use the ASG method to train their models, perhaps momentum schedules incorporating negative values towards the end of training can improve performance.

Acknowledgements

We thank Leon Bottou, Aaron Defazio, Alexandre Defossez, Tom Goldstein, and Mark Tygert for feedback and conversations about earlier versions of this work.

References

- Allen-Zhu, Z. Katyusha: The first direct acceleration of stochastic gradient methods. *The Journal of Machine Learning Research*, 18(1):8194–8244, 2017.
- Allen-Zhu, Z. and Orecchia, L. Linear coupling: An ultimate unification of gradient and mirror descent. *arXiv preprint arXiv:1407.1537*, 2014.
- Aybat, N. S., Fallah, A., Gürbüzbalaban, M., and Ozdaglar, A. Robust accelerated gradient methods for smooth strongly convex functions. Nov. 2019.
- Bottou, L., Curtis, F. E., and Nocedal, J. Optimization methods for large-scale machine learning. *SIAM Review*, 60(2):223–311, 2018.

- Bubeck, S. Convex optimization: Algorithms and complexity. *Foundations and Trends in Machine Learning*, 8(3-4): 231–357, 2015.
- Can, B., Gurbuzbalaban, M., and Zhu, L. Accelerated linear convergence of stochastic momentum methods in wasserstein distances. *arXiv preprint arXiv:1901.07445*, 2019.
- Cohen, M. B., Diakonikolas, J., and Orecchia, L. On acceleration with noise-corrupted gradients. In *International Conference on Machine Learning (ICML)*, 2018.
- d'Aspremont, A. Smooth optimization with approximate gradient. *SIAM Journal on Optimization*, 19(3):1171–1183, 2008.
- Defazio, A. On the curved geometry of accelerated optimization. In *Advances in Neural Information Processing Systems*, pp. 1764–1773, 2019.
- Devolder, O., Glineur, F., and Nesterov, Y. First-order methods of smooth convex optimization with inexact oracle. *Mathematical Programming*, 146(1–2):37–75, 2014.
- Ghadimi, S. and Lan, G. Optimal stochastic approximation algorithms for strongly convex stochastic composite optimization I: A generic algorithmic framework. *SIAM Journal of Optimization*, 22(4), 2012.
- Ghadimi, S. and Lan, G. Optimal stochastic approximation algorithms for strongly convex stochastic composite optimization II: Shrinking procedures and optimal algorithms. *SIAM Journal of Optimization*, 23(4), 2013.
- Gidel, G., Hemmat, R. A., Pezeshki, M., Lepriol, R., Huang, G., Lacoste-Julien, S., and Mitliagkas, I. Negative momentum for improved game dynamics. *arXiv preprint arXiv:1807.04740*, 2018.
- Gitman, I., Lang, H., Zhang, P., and Xiao, L. Understanding the role of momentum in stochastic gradient methods. In *Advances in Neural Information Processing Systems*, pp. 9630–9640, 2019.
- Gower, R., Loizou, N., Qian, X., Sailanbayev, A., Shulgin, E., and Richtarik, P. SGD: General analysis and improved rates. In *International Conference on Machine Learning*, pp. 5200–5209, 2019.
- Horn, R. A. and Johnson, C. R. *Matrix Analysis*. Cambridge University Press, 2nd edition, 2013.
- Hu, B. and Lessard, L. Dissipativity theory for Nesterov's accelerated method. In *Proceedings of the 34th International Conference on Machine Learning-Volume 70*, pp. 1549–1557. JMLR. org, 2017.
- Kidambi, R., Netrapalli, P., Jain, P., and Kakade, S. M. On the insufficiency of existing momentum schemes for stochastic optimization. In *International Conference on Learning Representations*, 2018.
- Kulunchakov, A. and Mairal, J. Estimate sequences for variance-reduced stochastic composite optimization. In *International Conference on Machine Learning*, 2019a.
- Kulunchakov, A. and Mairal, J. A generic acceleration framework for stochastic composite optimization. In *Advances in Neural Information Processing Systems*, 2019b.
- Laborde, M. and Oberman, A. A Lyapunov analysis for accelerated gradient methods: From deterministic to stochastic case. Sep. 2019.
- Lan, G. An optimal method for stochastic composite optimization. *Mathematical Programming*, 133(1-2):365–397, 2012.
- Lenard, M. L. and Minkoff, M. Randomly generated test problems for positive definite quadratic programming. *ACM Transactions on Mathematical Software (TOMS)*, 10(1):86–96, 1984.
- Lessard, L., Recht, B., and Packard, A. Analysis and design of optimization algorithms via integral quadratic constraints. *SIAM Journal on Optimization*, 26(1):57–95, 2016.
- Liu, C. and Belkin, M. Accelerating SGD with momentum for over-parameterized learning. In *International Conference on Learning Representations*, 2020.
- Loizou, N. and Richtárik, P. Momentum and stochastic momentum for stochastic gradient, newton, proximal point and subspace descent methods. *arXiv preprint arXiv:1712.09677*, 2017.
- Ma, J. and Yarats, D. Quasi-hyperbolic momentum and adam for deep learning. In *International Conference on Learning Representations*, 2019.
- Ma, S., Bassily, R., and Belkin, M. The power of interpolation: Understanding the effectiveness of SGD in modern over-parameterized learning. In *International Conference on Machine Learning*, 2018.
- Mitliagkas, I., Zhang, C., Hadjis, S., and Ré, C. Asynchrony begets momentum, with an application to deep learning. In *2016 54th Annual Allerton Conference on Communication, Control, and Computing (Allerton)*, pp. 997–1004. IEEE, 2016.
- Nesterov, Y. A method for solving a convex programming problem with convergence rate $\mathcal{O}(1/k^2)$. *Soviet Mathematics Doklady*, 27:372–367, 1983.

- Nesterov, Y. Introductory lectures on convex optimization: a basic course. *Kluwer Academic Publishers*, pp. 71–81, 2004.
- O'Donoghue, B. and Candès, E. Adaptive restart for accelerated gradient schemes. *Foundations of computational mathematics*, 15(3):715–732, 2015.
- Pedregosa, F., Varoquaux, G., Gramfort, A., Michel, V., Thirion, B., Grisel, O., Blondel, M., Prettenhofer, P., Weiss, R., Dubourg, V., Vanderplas, J., Passos, A., Cournapeau, D., Brucher, M., Perrot, M., and Duchesnay, E. Scikit-learn: Machine learning in Python. *Journal of Machine Learning Research*, 12:2825–2830, 2011.
- Polyak, B. T. Some methods of speeding up the convergence of iteration methods. *USSR Computational Mathematics and Mathematical Physics*, 4(5):1–17, 1964.
- Polyak, B. T. *Introduction to Optimization*. Optimization Software Inc., 1987.
- Rota, G.-C. and Strang, W. A note on the joint spectral radius. 1960.
- Schmidt, M. and Le Roux, N. Fast convergence of stochastic gradient descent under a strong growth condition. Aug. 2013.
- Su, W., Boyd, S., and Candès, E. A differential equation for modeling nesterov's accelerated gradient method: Theory and insights. In *Advances in Neural Information Processing Systems*, pp. 2510–2518, 2014.
- Sutskever, I., Martens, J., Dahl, G., and Hinton, G. On the importance of initialization and momentum in deep learning. In *International conference on machine learning*, pp. 1139–1147, 2013.
- Vaswani, S., Bach, F., and Schmidt, M. Fast and faster convergence of SGD for over-parameterized models (and an accelerated perceptron). In *International Conference on Machine Learning*, 2019.
- Wiegerinck, W., Komoda, A., and Heskes, T. Stochastic dynamics of learning with momentum in neural networks. *Journal of Physics A: Mathematical and General*, 27(13): 4425, 1994.
- Yang, T., Lin, Q., and Li, Z. Unified convergence analysis of stochastic momentum methods for convex and non-convex optimization. *arXiv preprint arXiv:1604.03257*, 2016.

Supplementary Material for On the Convergence of Nesterov's Accelerated Gradient Method in Stochastic Settings

A. Proof of Theorem 1

We begin from (14). By taking the squared norm on both sides, and recalling that the random vectors ζ_k have zero mean and are mutually independent, we have

$$\begin{aligned}
\mathbb{E} \|y_{k+1} - x^*\|^2 &\leq \mathbb{E} \left\| \begin{bmatrix} r_{k+1} \\ v_k \end{bmatrix} \right\|^2 \\
&= \mathbb{E}_{\zeta_k, \dots, \zeta_1} \left\| A^k \begin{bmatrix} x_1 - x^* \\ 0 \end{bmatrix} - \alpha \sum_{j=1}^k A^{k-j} \begin{bmatrix} (1+\beta)I \\ I \end{bmatrix} \zeta_j \right\|^2 \\
&= \mathbb{E}_{\zeta_k} \left[\dots \mathbb{E}_{\zeta_1} \left\| A^k \begin{bmatrix} x_1 - x^* \\ 0 \end{bmatrix} - \alpha \sum_{j=1}^k A^{k-j} \begin{bmatrix} (1+\beta)I \\ I \end{bmatrix} \zeta_j \right\|^2 \dots \right] \\
&= \left\| A^k \begin{bmatrix} x_1 - x^* \\ 0 \end{bmatrix} \right\|^2 + \alpha^2 \sum_{j=1}^k \mathbb{E}_{\zeta_j} \left\| A^{k-j} \begin{bmatrix} (1+\beta)I \\ I \end{bmatrix} \zeta_j \right\|^2 \\
&\leq \|A^k\|^2 \|x_1 - x^*\|^2 + \alpha^2 ((1+\beta)^2 + 1) \sigma^2 \sum_{j=1}^k \|A^{k-j}\|^2. \tag{25}
\end{aligned}$$

Recall that the spectral radius of a square matrix $A \in \mathbb{R}^{2d \times 2d}$ is defined as $\max_{i=1, \dots, 2d} |\lambda_i(A)|$, where $\lambda_i(A)$ is the i th eigenvalue of A . The spectral radius satisfies (Horn & Johnson, 2013)

$$\rho(A)^k \leq \|A^k\| \quad \text{for all } k,$$

and (Gelfand's theorem)

$$\lim_{k \rightarrow \infty} \|A^k\|^{1/k} = \rho(A).$$

Hence, for any $\epsilon > 0$, there exists a K_ϵ such that $\|A^k\|^{1/k} \leq (\rho(A) + \epsilon)$ for all $k \geq K_\epsilon$. Let

$$C_\epsilon = \max_{k < K_\epsilon} \max \left\{ 1, \frac{\|A^k\|}{(\rho(A) + \epsilon)^k} \right\}. \tag{26}$$

Then $\|A^k\| \leq C_\epsilon (\rho(A) + \epsilon)^k$ for all k . Moreover, if $\|A^k\|^{1/k}$ converges monotonically to $\rho(A)$, then $C_\epsilon \leq \|A\| / \rho(A)$.

Now, recall that we have assumed $f(x) = \frac{1}{2} x^\top H x - b^\top x + c$ where $H \in \mathbb{R}^{d \times d}$ is symmetric, and we have also assumed that f is L -smooth and μ -strongly convex. Thus all eigenvalues of H satisfy $\mu \leq \lambda_i(H) \leq L$.

Lemma 2. For A as defined in (15), we have $\rho(A) = \max\{\rho_\mu(\alpha, \beta), \rho_L(\alpha, \beta)\}$ where

$$\rho_\lambda(\alpha, \beta) = \begin{cases} \frac{1}{2} |(1+\beta)(1-\alpha\lambda)| + \frac{1}{2} \sqrt{\Delta_\lambda} & \text{if } \Delta_\lambda \geq 0, \\ \sqrt{\beta(1-\alpha\lambda)} & \text{otherwise,} \end{cases}$$

and $\Delta_\lambda = (1+\beta)^2(1-\alpha\lambda)^2 - 4\beta(1-\alpha\lambda)$.

Proof. Since H is real and symmetric, it has a real eigenvalue decomposition $H = U\Lambda_H U^\top$, where $U \in \mathbb{R}^{d \times d}$ is an orthogonal matrix and Λ_H is the diagonal matrix of eigenvalues of H . Observe that A can be viewed as a 2×2 block matrix with $d \times d$ blocks that all commute with each other, since each block is an affine matrix function of H . Thus, by Polyak (1964, Lemma 5), ξ is an eigenvalue of A if and only if there is an eigenvalue λ of H , such that ξ is an eigenvalue of the 2×2 matrix

$$B(\lambda) := \begin{bmatrix} 1 - \alpha(1 + \beta)\lambda & \beta^2 \\ -\alpha\lambda & \beta \end{bmatrix}. \quad (27)$$

The characteristic polynomial of $B(\lambda)$ is

$$\xi^2 - (1 + \beta)(1 - \alpha\lambda)\xi + \beta(1 - \alpha\lambda) = 0,$$

from which it follows that eigenvalues of $B(\lambda)$ are given by $\rho_\lambda(\alpha, \beta)$; see, e.g., Lessard et al. (2016, Appendix A). Note that the characteristic polynomial of $B(\lambda)$ is the same as the characteristic polynomial of a different matrix appearing in Lessard et al. (2016), that arises from a different analysis of the AG method. Finally, as discussed in Lessard et al. (2016), for any fixed values of α and β , the function $\rho_\lambda(\alpha, \beta)$ is quasi-convex in λ , and hence the maximum over all eigenvalues of A is achieved at one of the extremes $\lambda = \mu$ or $\lambda = L$. \square

To complete the proof of Theorem 1, use Lemma 2 with (25) to obtain that, for any $\epsilon > 0$, there is a positive constant C_ϵ such that

$$\begin{aligned} \mathbb{E}[\|y_{k+1} - x^*\|^2] &\leq C_\epsilon \left((\rho(A) + \epsilon)^{2k} \|x_0 - x^*\|^2 + \alpha^2((1 + \beta)^2 + 1)\sigma^2 \sum_{j=1}^k (\rho(A) + \epsilon)^{2(k-j)} \right) \\ &\leq C_\epsilon \left((\rho(A) + \epsilon)^{2k} \|x_0 - x^*\|^2 + \frac{\alpha^2((1 + \beta)^2 + 1)}{1 - (\rho(A) + \epsilon)^2} \sigma^2 \right). \end{aligned}$$

A.1. Estimating the constant C_ϵ

For the theoretical plots in the numerical experiments in Section 3.2 and in Appendix G below, we estimate the constant C_ϵ by taking $K_\epsilon \approx 2$ in (26). That is, for arbitrarily small ϵ and all $k \geq 2$, we approximate $\|A^k\|^{1/k}$ by $(\rho(A) + \epsilon)$. Therefore, the summation term in (25) is approximated as

$$\alpha^2((1 + \beta)^2 + 1) \left(\frac{1}{1 - \rho(\alpha, \beta)^2} + (\|A\|^2 - \rho(\alpha, \beta)^2) \right), \quad (28)$$

where $\|A\|$ denotes the largest singular value of A in (15), and $\rho(\alpha, \beta)$ is the largest eigenvalue of A . The first term in (28) corresponds to the geometric limit of the summation term in (25) after taking matrix norms and approximating the norms of matrix products by powers of the spectral radius for all products $k \geq 2$. The difference term in (28) is simply used to correct for the case $k = 1$. Setting $C_\epsilon \frac{\alpha^2((1 + \beta)^2 + 1)}{1 - \rho(\alpha, \beta)^2}$ equal to (28) and solving for C_ϵ gives us the approximate expression for C_ϵ used in the theoretical plots in Section 3.2.

B. Proofs of Corollary 1.1 and Theorem 2

Taking $\alpha = 1/L$ and $\beta = \frac{\sqrt{Q}-1}{\sqrt{Q+1}}$, we find that $\rho(\alpha, \beta) = \frac{\sqrt{Q}-1}{\sqrt{Q}}$. Since $f(x) = \frac{1}{2}x^T Hx - b^T x + c$ is an L -smooth μ -strongly convex quadratic, all eigenvalues of H are bounded between μ and L . Therefore, from Polyak (1964, Lemma 5), we have that $\|A^k\|_2 \leq \max_{\lambda \in [\mu, L]} \|B(\lambda)^k\|_2 \leq \max_{\lambda \in [\mu, L]} \sqrt{d} \|B(\lambda)^k\|_\infty$, where $B(\lambda)$ is as defined in (27). The eigenvalues of $B(\lambda)^k$ are maximized at $\lambda = \mu$ for $k > 1$, therefore, for large k , $\|B(\lambda)^k\|_\infty$ is maximized at $\lambda = \mu$.

Note that the Jordan form of $B(\mu)$ is given by VJV^{-1} , where

$$V = \begin{bmatrix} \frac{\sqrt{Q}(\sqrt{Q}-1)}{\sqrt{Q+1}} & Q \\ -1 & 0 \end{bmatrix} \quad \text{and} \quad J = \begin{bmatrix} \frac{\sqrt{Q}-1}{\sqrt{Q}} & 1 \\ 0 & \frac{\sqrt{Q}-1}{\sqrt{Q}} \end{bmatrix}.$$

Using the Jordan form, we determine that $B(\mu)^k$ is

$$B(\mu)^k = \begin{bmatrix} \left(1 + \frac{k}{\sqrt{Q+1}}\right) \left(\frac{\sqrt{Q}-1}{\sqrt{Q}}\right)^k & k \left(\frac{\sqrt{Q}-1}{\sqrt{Q+1}}\right)^2 \left(\frac{\sqrt{Q}-1}{\sqrt{Q}}\right)^{k-1} \\ -\frac{k}{Q} \left(\frac{\sqrt{Q}-1}{\sqrt{Q}}\right)^{k-1} & \left(1 - \frac{k}{\sqrt{Q+1}}\right) \left(\frac{\sqrt{Q}-1}{\sqrt{Q}}\right)^k \end{bmatrix}.$$

Therefore, we have that

$$\|B(\mu)^k\|_\infty \leq \left(1 + \frac{k}{\sqrt{Q+1}}\right) \left(\frac{\sqrt{Q}-1}{\sqrt{Q}}\right)^k + k \max \left\{ \frac{1}{Q}, \left(\frac{\sqrt{Q}-1}{\sqrt{Q+1}}\right)^2 \right\} \left(\frac{\sqrt{Q}-1}{\sqrt{Q}}\right)^{k-1}. \quad (29)$$

Therefore for large k

$$\|A^k\|_2^2 \leq d \|B(\mu)^k\|_\infty^2 = \left(\frac{\sqrt{Q}-1}{\sqrt{Q}} + \epsilon_k\right)^{2k},$$

where $\epsilon_k \sim (\sqrt[k]{k} - 1)$. Also observe that

$$\begin{aligned} \frac{\alpha^2((1+\beta)^2+1)}{1-\rho(\alpha,\beta)^2} &= \frac{1}{L^2} \frac{\left(\frac{2\sqrt{Q}}{\sqrt{Q+1}}\right)^2 + 1}{1 - \left(\frac{\sqrt{Q}-1}{\sqrt{Q}}\right)^2} \\ &= \frac{1}{L^2} \frac{5Q^2 + 2Q^{3/2} + Q}{(\sqrt{Q}+1)^2(2\sqrt{Q}-1)}. \end{aligned}$$

Since f is L -smooth,

$$f(y_{k+1}) - f^* \leq \frac{L}{2} \|y_{k+1} - x^*\|^2.$$

Thus, by Theorem 1 we have

$$\mathbb{E}[f(y_{k+1})] - f^* \leq \frac{L}{2} \left(\frac{\sqrt{Q}-1}{\sqrt{Q}} + \epsilon_k\right)^{2k} \|x_0 - x^*\|^2 + C_\epsilon \frac{5Q^2 + 2Q^{3/2} + Q}{2L(2\sqrt{Q}-1)(\sqrt{Q}+1)^2} \sigma^2,$$

which completes the proof of Corollary 1.1.

To prove Theorem 2, first observe that when $\beta = 0$, the recursion simplifies significantly. Specifically, then $y_{k+1} = x_k$, $v_k = -\alpha g_k$, and we have (using similar notation as in the proof of Theorem 1)

$$\begin{aligned} r_{k+1} &= (I - \alpha H_k) r_k - \alpha \zeta_k \\ &= \prod_{j=1}^k (I - \alpha H_j) r_1 - \alpha \zeta_k - \alpha \sum_{j=1}^{k-1} \prod_{l=j+1}^k (I - \alpha H_l) \zeta_j, \end{aligned}$$

where

$$H_j = \int_0^1 \nabla f^2(x^* - t r_j) dt.$$

Of course, since f is L -smooth and μ -strongly convex, all eigenvalues of H_j lie in the interval $[\mu, L]$ for all $j \geq 0$.

Now, taking the squared norm on both sides, and recalling that the random vectors ζ_k have zero mean and are mutually

independent, we have

$$\begin{aligned}
 \mathbb{E} \|y_{k+1} - x^*\|^2 &= \mathbb{E} \|r_{k+1}\|^2 \\
 &= \mathbb{E}_{\zeta_k, \dots, \zeta_1} \left\| \prod_{j=1}^k (I - \alpha H_j) r_1 - \alpha \zeta_k - \alpha \sum_{j=1}^{k-1} \prod_{l=j+1}^k (I - \alpha H_l) \zeta_j \right\|^2 \\
 &= \mathbb{E}_{\zeta_k} \left[\dots \mathbb{E}_{\zeta_1} \left[\left\| \prod_{j=1}^k (I - \alpha H_j) r_1 - \alpha \zeta_k - \alpha \sum_{j=1}^{k-1} \prod_{l=j+1}^k (I - \alpha H_l) \zeta_j \right\|^2 \right] \dots \right] \\
 &= \left(\prod_{j=1}^k \|I - \alpha H_j\|^2 \right) \|x_1 - x^*\|^2 + \alpha^2 \mathbb{E}_{\zeta_k} \|\zeta_k\|^2 + \alpha^2 \sum_{j=1}^{k-1} \mathbb{E}_{\zeta_j} \left\| \left(\prod_{l=j+1}^k I - \alpha H_l \right) \zeta_j \right\|^2 \\
 &\leq \left(\prod_{j=1}^k \|I - \alpha H_j\|^2 \right) \|x_1 - x^*\|^2 + \alpha^2 \sigma^2 + \alpha^2 \sigma^2 \sum_{j=1}^{k-1} \left(\prod_{l=j+1}^k \|I - \alpha H_l\|^2 \right).
 \end{aligned}$$

Now, since $I - \alpha H_j$ is symmetric, we have $\|(I - \alpha H_j)\|^2 = \rho(I - \alpha H_j)^2$, where $\rho(I - \alpha H_j)$ denotes the spectral radius of $I - \alpha H_j$ (the largest magnitude of an eigenvalue of $I - \alpha H_j$). For $\alpha = \frac{2}{\mu+L}$, and since the eigenvalues of H_j lie in the interval $[\mu, L]$, it is straightforward to show that $\rho(I - \alpha H_j) = \frac{Q-1}{Q+1}$.

Therefore we have

$$\begin{aligned}
 \mathbb{E} \left[\|y_{k+1} - x^*\|^2 \right] &\leq \left(\frac{Q-1}{Q+1} \right)^{2k} \|x_0 - x^*\|^2 + \alpha^2 \sigma^2 \sum_{j=1}^k \left(\frac{Q-1}{Q+1} \right)^{2(k-j)} \\
 &\leq \left(\frac{Q-1}{Q+1} \right)^{2k} \|x_0 - x^*\|^2 + \frac{\alpha^2 \sigma^2}{1 - \left(\frac{Q-1}{Q+1} \right)^2} \\
 &= \left(\frac{Q-1}{Q+1} \right)^{2k} \|x_0 - x^*\|^2 + \frac{Q}{2L} \sigma^2,
 \end{aligned}$$

which completes the proof of Theorem 2.

C. Permutation Matrix Construction

For a vector $x \in \mathbb{R}^d$, let $\text{diag}(x)$ denote a $d \times d$ diagonal matrix with its i th diagonal entry equal to x_i . Let $a, b, c, d \in \mathbb{R}^d$ and suppose $M \in \mathbb{R}^{2d \times 2d}$ is the matrix

$$M = \begin{bmatrix} \text{diag}(a) & \text{diag}(b) \\ \text{diag}(c) & \text{diag}(d) \end{bmatrix}.$$

Let $P \in \{0, 1\}^{2d \times 2d}$ be the permutation matrix with entries $P_{i,j}$ for $i, j = 1, \dots, 2d$ given by

$$P_{i,j} = \begin{cases} 1 & \text{if } i \text{ is odd and } j = (i-1)/2 + 1 \\ 1 & \text{if } i \text{ is even and } j = d + \lfloor \frac{i-1}{2} \rfloor + 1 \\ 0 & \text{otherwise.} \end{cases}$$

Then one can verify that

$$PMP^\top = \begin{bmatrix} T_1 & 0 & \dots & 0 \\ 0 & T_2 & \dots & 0 \\ \vdots & \vdots & \ddots & \vdots \\ 0 & 0 & \dots & T_d \end{bmatrix}$$

where, for $j = 1, \dots, d$, T_j is the 2×2 matrix

$$T_j = \begin{bmatrix} a_j & b_j \\ c_j & d_j \end{bmatrix}.$$

D. Proof of Lemma 1

Recall that $\alpha = 1/L$ and $\beta = \frac{\sqrt{Q}-1}{\sqrt{Q}+1}$. For matrices of the form

$$T_k = B(L)B(\mu)^{k_1}B(L)B(\mu)^{k_2} \cdots B(L)B(\mu)^{k_s}B(L),$$

where

$$B(\lambda) = \begin{bmatrix} 1 - \alpha(1 + \beta)\lambda & \beta^2 \\ -\alpha\lambda & \beta \end{bmatrix},$$

we would like to show that the spectral radius $\rho(T_k)$ is equal to

$$\rho(T_k) = \left(\frac{\sqrt{Q}-1}{\sqrt{Q}} \right)^k \times k_1 k_2 \cdots k_s.$$

To see this, first note that the Jordan form of $B(\mu)$ is given by VJV^{-1} , where

$$V = \begin{bmatrix} \frac{\sqrt{Q}(\sqrt{Q}-1)}{\sqrt{Q}+1} & Q \\ -1 & 0 \end{bmatrix} \quad \text{and} \quad J = \begin{bmatrix} \frac{\sqrt{Q}-1}{\sqrt{Q}} & 1 \\ 0 & \frac{\sqrt{Q}-1}{\sqrt{Q}} \end{bmatrix}.$$

Using the Jordan form, we determine that $B(\mu)^{k_\ell}$ is

$$B(\mu)^{k_\ell} = \begin{bmatrix} \left(1 + \frac{k_\ell}{\sqrt{Q}+1}\right) \left(\frac{\sqrt{Q}-1}{\sqrt{Q}}\right)^{k_\ell} & k_\ell \left(\frac{\sqrt{Q}-1}{\sqrt{Q}+1}\right)^2 \left(\frac{\sqrt{Q}-1}{\sqrt{Q}}\right)^{k_\ell-1} \\ -\frac{k_\ell}{Q} \left(\frac{\sqrt{Q}-1}{\sqrt{Q}}\right)^{k_\ell-1} & \left(1 - \frac{k_\ell}{\sqrt{Q}+1}\right) \left(\frac{\sqrt{Q}-1}{\sqrt{Q}}\right)^{k_\ell} \end{bmatrix}.$$

Through direct matrix multiplication

$$B(L)B(\mu)^{k_\ell}B(L) = - \left(\frac{\sqrt{Q}-1}{\sqrt{Q}} \right)^{k_\ell+1} k_\ell B(L).$$

Therefore,

$$T_j = (-1)^{s-1} \left(\frac{\sqrt{Q}-1}{\sqrt{Q}} \right)^{k-1-k_s} k_1 k_2 \cdots k_{s-1} B(L) B(\mu)^{k_s}.$$

Finally, the spectral-radius of $B(L)B(\mu)^{k_s}$ is

$$\rho(B(L)B(\mu)^{k_s}) = \left(\frac{\sqrt{Q}-1}{\sqrt{Q}} \right)^{k_s+1} k_s,$$

and hence

$$\rho(T_k) = \left(\frac{\sqrt{Q}-1}{\sqrt{Q}} \right)^k k_1 k_2 \cdots k_s.$$

E. Proof of Theorem 4

Since the functions f_i are assumed to be twice continuously differentiable, by (10) we can express the mini-batch gradients as

$$g_k = \tilde{H}_k r_k + z_k, \tag{30}$$

where

$$\tilde{H}_k = \sum_{i=1}^n v_{k,i} \int_0^1 \nabla^2 f_i(x^* + tr_k) dt$$

and

$$z_k = \sum_{i=1}^n v_{k,i} \nabla f_i(x^*).$$

By convexity of norms,

$$\|z_k\| \leq \sum_{i=1}^n v_{k,i} \|\nabla f_i(x^*)\|.$$

Hence, taking expectations gives

$$\begin{aligned} \mathbb{E}_k[\|z_k\|] &\leq \frac{1}{n} \sum_{i=1}^n \|\nabla f_i(x^*)\| \\ &= \sigma. \end{aligned}$$

Using (30) in (9) and unrolling, we obtain

$$\begin{bmatrix} r_{k+1} \\ v_k \end{bmatrix} = A_k \cdots A_1 \begin{bmatrix} r_1 \\ v_0 \end{bmatrix} - \alpha \begin{bmatrix} (1+\beta)I \\ I \end{bmatrix} z_k - \alpha \sum_{j=1}^{k-1} (A_k \cdots A_{j+1}) \begin{bmatrix} (1+\beta)I \\ I \end{bmatrix} z_j, \quad (31)$$

where

$$A_k = \begin{bmatrix} I - \alpha(1+\beta)\tilde{H}_k & \beta^2 I \\ -\alpha\tilde{H}_k & \beta I \end{bmatrix}.$$

By submultiplicativity of matrix norms, $\|A_k \cdots A_{j+1}\| \leq \prod_{l=j+1}^k \|A_l\|$. Thus we turn our attention to bounding the spectral norm of A_k .

Lemma 3.

$$\|A_k\| \leq \max_{\lambda \in [\mu, L]} \|B(\lambda)\| = R(\alpha, \beta).$$

Proof. For all $k \geq 0$, every eigenvalue of \tilde{H}_k lies in the interval $[\mu, L]$, based on the assumption that each function f_i is L -smooth and μ -strongly convex. It follows from Polyak (1964, Lemma 5) that there exists an eigenvalue λ of \tilde{H}_k such that $\|A_k\|$ is equal to the spectral norm of

$$B(\lambda) = \begin{bmatrix} 1 - \alpha(1+\beta)\lambda & \beta^2 \\ -\alpha\lambda & \beta \end{bmatrix}.$$

We next compute $\|B(\lambda)\|$, which is equal to the square root of the largest eigenvalue of

$$B(\lambda)^\top B(\lambda) = \begin{bmatrix} (1 - \alpha(1+\beta)\lambda)^2 + \alpha^2\lambda^2 & \beta^2(1 - \alpha(1+\beta)\lambda) - \alpha\beta\lambda \\ \beta^2(1 - \alpha(1+\beta)\lambda) - \alpha\beta\lambda & \beta^2(\beta^2 + 1) \end{bmatrix}.$$

The characteristic polynomial of $B(\lambda)^\top B(\lambda)$ is

$$\xi^2 - C_\lambda(\alpha, \beta)\xi + \beta^2(1 - \alpha\lambda)^2 = 0,$$

where

$$C_\lambda(\alpha, \beta) = (1 - \alpha(1+\beta)\lambda)^2 + \alpha^2\lambda^2 + \beta^2(\beta^2 + 1).$$

The largest root of the characteristic polynomial is equal to

$$R_\lambda(\alpha, \beta)^2 = \frac{1}{2} \left(C_\lambda(\alpha, \beta) + \sqrt{C_\lambda(\alpha, \beta)^2 - 4\beta^2(1 - \alpha\lambda)^2} \right)$$

which is equal to $\|B(\lambda)\|^2$. Therefore

$$\|A_k\| \leq \max_{\lambda \in [\mu, L]} R_\lambda(\alpha, \beta).$$

□

Assume that α and β have been chosen so that $R(\alpha, \beta) < 1$. Then for all k and $j + 1$, $\|A_k \cdots A_{j+1}\| \leq \prod_{l=j+1}^k \|A_l\| \leq R(\alpha, \beta)^{k-j}$.

Taking the norm on both sides of (31) and using the triangle inequality, we have

$$\left\| \begin{bmatrix} r_{k+1} \\ v_k \end{bmatrix} \right\| \leq R(\alpha, \beta)^k \left\| \begin{bmatrix} r_1 \\ v_0 \end{bmatrix} \right\| + \alpha \sqrt{(1 + \beta)^2 + 1} \sum_{j=1}^k R(\alpha, \beta)^{k-j} \|z_k\|. \quad (32)$$

Taking the expectation gives

$$\mathbb{E}_k \|y_{k+1} - x^*\| \leq \mathbb{E}_k \left\| \begin{bmatrix} r_{k+1} \\ v_k \end{bmatrix} \right\| \quad (33)$$

$$\leq R(\alpha, \beta)^k \|x_0 - x^*\| + \frac{\alpha \sqrt{(1 + \beta)^2 + 1}}{1 - R(\alpha, \beta)^2} \sigma. \quad (34)$$

F. Proof of Corollaries 4.2 and 4.1

When $\beta = 0$, we have $y_{k+1} = x_k$ and $v_k = -\alpha g_k$ for all k . In this case we have

$$r_{k+1} = r_k - \alpha g_k.$$

Since the objectives f_i are twice continuously differentiable, the mini-batch gradients can again be written as (using the same notation as in the proof of Theorem 4)

$$g_k = \tilde{H}_k r_k + z_k.$$

Thus, with $A_k = I - \alpha \tilde{H}_k$, we have

$$\begin{aligned} r_{k+1} &= A_k r_k - \alpha z_k \\ &= A_k \cdots A_1 r_1 - \alpha z_k - \alpha \sum_{j=1}^{k-1} (A_k \cdots A_{j+1}) z_k. \end{aligned}$$

Since \tilde{H}_k is symmetric, it follows that A_k is also symmetric, and so $\|A_k\|$ is equal to the largest magnitude of any eigenvalue of A_k . Recall that all eigenvalues of \tilde{H}_k lie in the interval $[\mu, L]$. Therefore, $\|A_k\| \leq \max_{\lambda \in [\mu, L]} |1 - \alpha \lambda| = \max\{|1 - \alpha \mu|, |1 - \alpha L|\}$. Choosing $\alpha < \frac{2}{L}$ and taking the norm and expectation thus yields that

$$\begin{aligned} \mathbb{E}_k \|x_k - x^*\| &= \mathbb{E}_k \|r_{k+1}\| \\ &\leq \left| 1 - \alpha \tilde{\lambda} \right|^k \|x_0 - x^*\| + \frac{\alpha}{1 - \left| 1 - \alpha \tilde{\lambda} \right|} \sigma, \end{aligned} \quad (35)$$

where $\tilde{\lambda} := \operatorname{argmax}_{\lambda \in \{\mu, L\}} |1 - \alpha \lambda|$. When $\alpha = \frac{2}{\mu + L}$, we have that $\max_{\lambda \in [\mu, L]} |1 - \alpha \lambda| = \frac{Q-1}{Q+1}$, and equation (35) simplifies as

$$\begin{aligned} \mathbb{E}_k \|x_k - x^*\| &= \mathbb{E}_k \|r_{k+1}\| \\ &\leq \left(\frac{Q-1}{Q+1} \right)^k \|x_0 - x^*\| + \frac{1}{\mu} \sigma. \end{aligned}$$

G. Additional Experiments

G.1. Least Squares

To provide additional experiments illustrating the relationship between empirical observations and the theory developed in Section 3 for the stochastic approximation setting, we conduct additional experiments on randomly-generated least-squares problems. We generate the least-squares problem using the approach described in (Lenard & Minkoff, 1984). Visualizations are shown in Figure G.1.

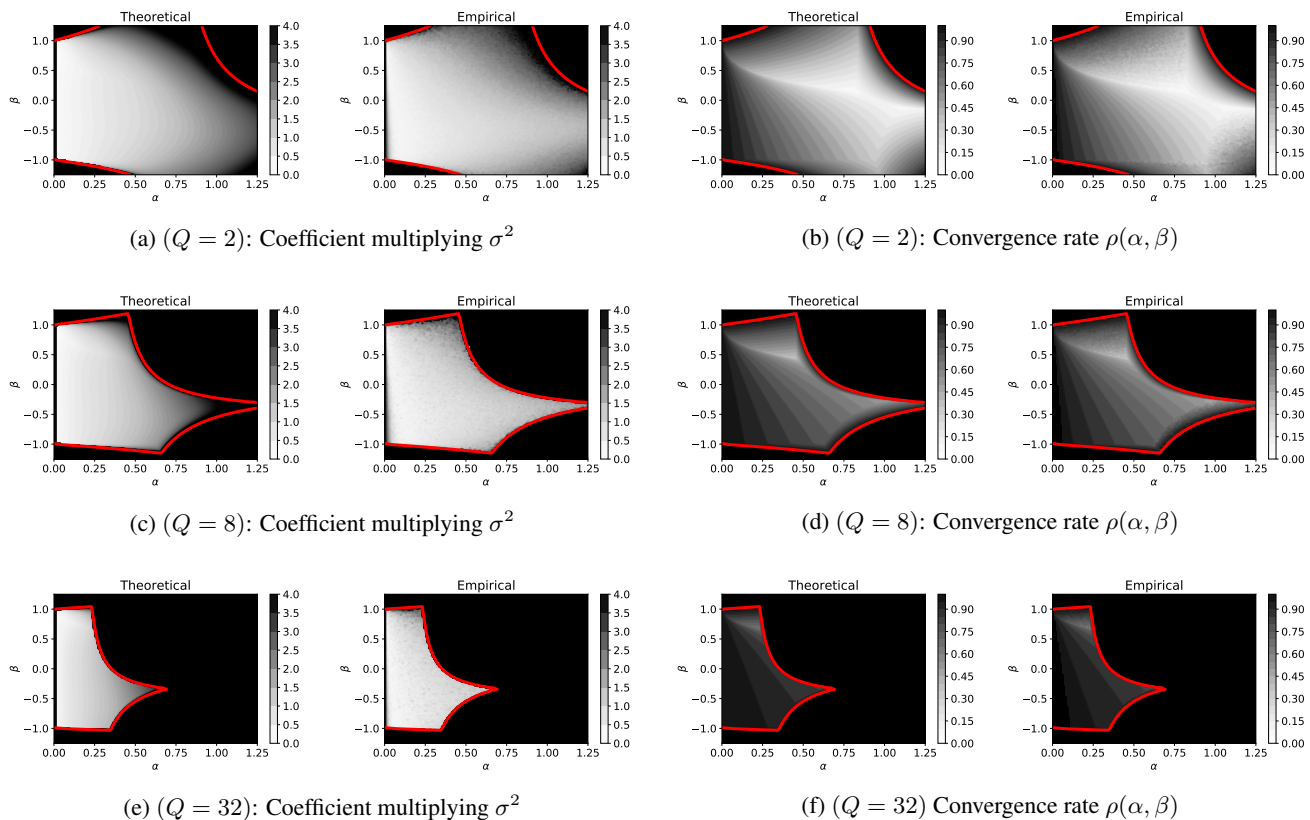


Figure G.1. Visualizing the accuracy with which the theory predicts the coefficient of the variance term and the convergence rate for different choices of constant step-size and momentum parameters, and various objective condition numbers Q . Plots labeled “Theoretical” depict theoretical results from Theorem 1. Plots labeled “Empirical” depict empirical results when using the ASG method to solve a least-squares regression problem with additive Gaussian noise; each pixel corresponds to an independent run of the ASG method for a specific choice of constant step-size and momentum parameters. In all figures, the area enclosed by the red contour depicts the theoretical stability region from Theorem 1 for which $\rho(\alpha, \beta) < 1$. Fig. G.1a/G.1c/G.1e: Pixel intensities correspond to the coefficient of the variance term in Theorem 1 ($\lim_{k \rightarrow \infty} \frac{1}{\sigma} \mathbb{E} \|y_k - x^*\|_\infty$), which provides a good characterization of the magnitude of the neighbourhood of convergence, even without explicit knowledge of the constant C_ϵ . Fig. G.1b/G.1d/G.1f: Pixel intensities correspond to the theoretical convergence rates in Theorem 1, which provides a good characterization of the empirical convergence rates. Moreover, the theoretical conditions for convergence in Theorem 1 depicted by the red-contour are tight.

We run the ASG method on least-squares regression problems with various condition numbers Q . The objectives f correspond to randomly generated least squares problems, consisting of 500 data samples with 10 features each. Stochastic gradients are sampled by adding zero-mean Gaussian noise, with standard-deviation $\sigma = 0.25$, to the true gradient. The left plots in each sub-figure depict theoretical predictions from Theorem 1, while the right plots in each sub-figure depict empirical results. Each pixel corresponds to an independent run of the ASG method for a specific choice of constant step-size and momentum parameters. In all figures, the area enclosed by the red contour depicts the theoretical stability region from Theorem 1 for which $\rho(\alpha, \beta) < 1$.

Figures G.1a/G.1c/G.1e showcase the coefficient multiplying the variance term, which is taken to be $\frac{\alpha^2((1+\beta)^2+1)}{1-\rho(\alpha,\beta)^2}$ in theory. Brighter regions correspond to smaller coefficients, while darker regions correspond to larger coefficients. All sets of figures (theoretical and empirical) use the same color scale. We can see that the coefficient of the variance term in Theorem 1 provides a good characterization of the magnitude of the neighbourhood of convergence. The constant C_ϵ is approximated as $1 + (1 - \rho(\alpha, \beta)^2)(\varrho(\alpha, \beta)^2 - \rho(\alpha, \beta)^2)$, where $\varrho(\alpha, \beta)$ is defined as the largest singular value of A in (15), and $\rho(\alpha, \beta)$ is the largest eigenvalue of A .

Figures. G.1b/G.1d/G.1f showcase the linear convergence rate in theory and in practice. Brighter regions correspond to

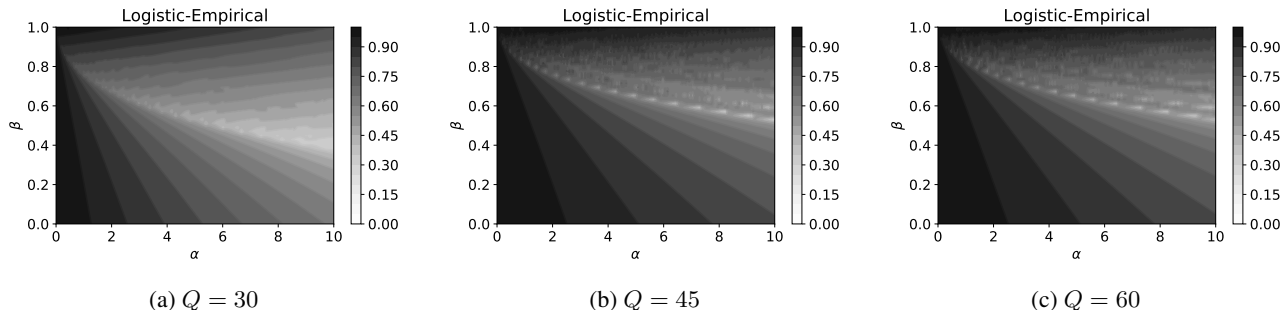


Figure G.2. Visualizing the convergence rate for the ASG method (momentum $\beta > 0$) and the SGD method (momentum $\beta = 0$), for various randomly generated ℓ_2 regularized multinomial logistic-regression problems. Multi-class classification problems consist of 5 classes and 100 data samples with 10 features each, only 5 of which are discriminative. We create one data-cluster per class, and vary the cluster separation and regularization parameter to vary the condition number Q . For reporting purposes, we estimate the condition number Q during training by evaluating the eigenvalues of the Hessian at each iteration. The smoothness constant L is taken to be the maximum eigenvalue seen during training, and the modulus of strong-convexity μ is taken to be the minimum eigenvalue seen during training. The faster convergence rates (brighter regions) correspond to $\beta > 0$, indicating that the ASG method provides acceleration over SGD in this stochastic approximation setting. Moreover, for a given step-size, the contrast between the brighter regions ($\beta > 0$) and darker regions ($\beta = 0$) increases as the condition number grows, supporting theoretical findings that the convergence rate of the ASG method exhibits a better dependence on the condition number than SGD.

faster rates, and darker regions correspond to slower rates. Again, all figures (theoretical and empirical) use the same color scale. We can see that the theoretical linear convergence rates in Theorem 1 provide a good characterization of the empirical convergence rates. Moreover, the theoretical conditions for convergence in Theorem 1 depicted by the red-contour appear to be tight.

G.2. Multinomial Logistic Regression

Next we conduct experiments on ℓ_2 regularized multinomial logistic regression problems with additive Gaussian noise, to examine whether the ASG method still achieves acceleration over SGD for these problems in the stochastic approximation setting, as is predicted by the theory in Section 3. These problems are smooth and strongly-convex, but non-quadratic. Tight estimates of the smoothness constant L and the modulus of strong-convexity μ cannot be computed definitively since the eigenvalues of the Hessian vary throughout the parameter space.

We randomly generate multi-class classification problems consisting of 5 classes and 100 data samples with 10 features each, only five of which are discriminative. We create one data cluster per class, and vary the cluster separation and regularization parameter to vary the condition number Q . For reporting purposes, we estimate the condition number Q during training by evaluating the eigenvalues of the Hessian at each iteration. The smoothness constant L is taken to be the maximum eigenvalue seen during training, and the modulus of strong-convexity μ is taken to be the minimum eigenvalue seen during training. We use the `make_classification()` function in scikit-learn (Pedregosa et al., 2011) to generate random classification problem instances.

Visualizations are provided in Figure G.2. Each pixel corresponds to an independent run of the ASG method for a specific choice of constant step-size and momentum parameters. Pixel intensities denote the linear convergence rates observed in practice. Brighter regions correspond to faster rates, and darker regions correspond to slower rates.

The parameter setting β equals 0 corresponds to SGD, and the parameter setting $\beta > 0$ corresponds to the ASG method. The faster convergence rates (brighter regions) correspond to $\beta > 0$, indicating that the ASG method provides acceleration over SGD in this stochastic approximation setting. Moreover, for a given step-size, the contrast between the brighter regions ($\beta > 0$) and darker regions ($\beta = 0$) increases as the condition number grows, supporting theoretical findings that the convergence rate of the ASG method exhibits a better dependence on the condition number than SGD.